Journal of Orthopaedic Translation 33 (2022) 13–23

Contents lists available at ScienceDirect

Journal of Orthopaedic Translation

journal homepage: www.journals.elsevier.com/journal-of-orthopaedic-translation

3D gel-printed porous magnesium scaffold coated with dibasic calcium phosphate dihydrate for bone repair in vivo☆

Yuxuan Zhang [a,c,1], Tao Lin [b,1], Haoye Meng [c,1], Xueting Wang [c], Hong Peng [a], Guangbo Liu [a,d], Shuai Wei [e], Qiang Lu [c], Yu Wang [c], Aiyuan Wang [c], Wenjing Xu [c], Huiping Shao [b,**], Jiang Peng [c,*]

[a] Medical School of Chinese PLA, Beijing, 100853, China
[b] Institute for Advanced Materials & Technology, University of Science and Technology Beijing, Beijing, 100083, China
[c] Institute of Orthopedics, Chinese PLA General Hospital, Beijing Key Laboratory (No BZ0128), Beijing Key Lab of Regenerative Medicine in Orthopedics, Key Laboratory of Musculoskeletal Trauma & War Injuries PLA, Beijing, 100853, China
[d] Strategic Support Force Medical Center, No.9, Anxiang Beli, Beijing, 100101, China
[e] Tianjin Hospital, Tianjin University, No. 406 Jiefang South Road, Tianjin, 300211, China

ARTICLE INFO

Keywords:
Magnesium scaffold
Osteoanagenesis
Bone defect
Dicalcium phosphate dihydrate coating
Biodegradation

ABSTRACT

*Background: /*Objective: The treatment of bone defect has always been a difficult problem in orthopedic clinic. The search for alternative biodegradable implants is a hot topic. The development of biodegradable magnesium scaffolds for the treatment of bone defects has long been a goal of the public.

Methods: In this study, we proposed a porous magnesium scaffold prepared by 3D gel printing and surface modification with an additional calcium phosphate coating and use of its strength, degradability and slow degradation rate in a bone graft substitute material. The porous magnesium granular scaffold was prepared by 3D gel printing technology and modified by DCPD (Dibasic Calcium Phosphate Dihydrate) coating. The biocompatibility, degradation rate, and osteogenic ability of the scaffold were evaluated in vitro and in vivo.

Results: The biocompatibility, in vivo degradation and bone defect healing response of the implants were investigated. Porous magnesium scaffolds were successfully prepared, and the strength of sintered scaffolds reached 5.38 MPa. The degradation rates of scaffolds were significantly reduced after coating with DCPD. The cell compatibility evaluation showed that DCPD-coated Mg scaffold was suitable for cell proliferation. In vivo biosafety monitoring showed that scaffold implantation did not cause an increase in Mg ion concentration in vivo, and no toxic damage was detected in the liver or kidney. Micro-CT and pathological results showed that a large amount of new bone was formed at 6 weeks. At 12 weeks, approximately 52% of the scaffold volume remained. At 24 weeks, osteogenesis, which was stimulated by some residual scaffold, still can be observed. In summary, this study suggests that 3D gel-printed DCPD-coated porous magnesium scaffolds have great potential as bone graft alternatives.

Conclusion: In summary, this study suggests that 3D gel-printed DCPD-coated porous magnesium scaffolds have great potential as bone graft alternatives.

The Translational potential of this article: The translational potential of this article is to make use of the advantages of 3D gel printing technology with higher efficiency and lower cost compared with SLM and SLS technologies, and use pure magnesium powder as raw material to prepare degradable porous magnesium metal scaffolds, opening up a new technical route for the preparation of degradable porous magnesium scaffolds which are made for bone defect regeneration in the future.

☆ The work was performed at Institute of Orthopedics, Chinese PLA General Hospital, Beijing Key Laboratory (No BZ0128), Beijing Key Lab of Regenerative Medicine in Orthopedics, Key Laboratory of Musculoskeletal Trauma & War Injuries PLA.

* Corresponding author.
** Corresponding author.
E-mail addresses: 51013685@qq.com (Y. Zhang), lintao@ustb.edu.cn (T. Lin), menghaoye@126.com (H. Meng), 15871744797@163.com (X. Wang), kobe0215@163.com (H. Peng), dr_liuguangbo@126.com (G. Liu), weishuai0604@163.com (S. Wei), luqiangbj@163.com (Q. Lu), wangwangdian628@126.com (Y. Wang), wangaiyuan301@126.com (A. Wang), wenjingkitty@163.com (W. Xu), shaohp@ustb.edu.cn (H. Shao), pengjiang301@126.com (J. Peng).
[1] Co-first author: The first three authors contributed equally to this work and are considered as co-first author.

https://doi.org/10.1016/j.jot.2021.11.005
Received 20 July 2021; Received in revised form 7 November 2021; Accepted 16 November 2021

1. Introduction

Bone defects involve the loss of normal bone due to various reasons, such as trauma caused by traffic accidents and production safety accidents, tumors, infections, heredity, and surgery [1]. Bone defects constitute a major difficulty in clinical treatments of orthopedic patients and still present major clinical and socioeconomic problems. Previous studies have shown that more than 1 million bone grafts are performed in the United States alone every year, which represents the second most common tissue transplantation after blood transfusion [2,3]. At present, most clinical practice is still based on surgical implantation of bone repair material. Bone restorative materials can be divided into autograft, allograft, and bone graft substitutes.

Autologous bone transplantation is considered the gold standard in the treatment of bone defects [4]. However, this method is limited by the amount of bone in the patient's own donor area and cannot be used when the defect volume exceeds the range that the patient can provide. Moreover, defects of the donor site affect the appearance and even cause depression [5,6]. Allogeneic bone and allogeneic bone grafts have the risk of high failure rates, immune rejection and disease transmission [7]. Distraction osteogenesis requires a long time, which brings inconvenience to patients' lives and even leads to infection [8]. These disadvantages prevent it from being used widely. The search for new bone graft substitutes has gradually become the focus of new development [9]. Currently, materials used as bone graft substitutes mainly include bioceramics [8], various polymer materials [10], metal materials [11,12], and so forth.

Bioceramics include hydroxyapatite and calcium phosphate, which have good biocompatibility, bioactivity and bone conductivity [13,14]. Experiments have shown that bioceramic scaffolds have good repairability and can be used with various cancellous bone defects [15,16]. However, how to improve the mechanical properties of bioceramics and obtain degradation rates matching the rate of tissue regeneration so as to improve the biosafety of composites should be investigated in further studies [17]. Polymer materials mainly include polylactic acid, polyacetic acid and related derivative composite materials. Composite fibrous scaffolds prepared with these materials exhibit good hydrophilicity, improve cell adhesion and proliferation, and significantly enhance osteogenesis [18]. Due to the insufficient mechanical properties of bioceramics and polymer materials, deformation and brittle fracture are prone to occur [19]. Metallic materials such as titanium and its alloys are commonly used for load-bearing components such as with spinal defects [20]. However, with increasing implantation time, metal ions enter human tissues and cause damage to the host under the corrosive effect of body fluids on the Ti scaffold, ultimately leading to implantation failure [21]. For the above reasons, the development of a new generation of bone graft substitutes with good mechanical properties, biocompatibility, promotion of bone regeneration and degradability has become an area of interest.

As a biodegradable metal, magnesium and its alloys have attracted increasing attention [22]. Magnesium is the main cation in human cells and plays an important role in human metabolism. In virtue of its similar mechanical properties with those of bone, it can effectively link the stress shielding effect, and be degraded completely by body fluids. After implantation, it can be metabolized and excreted by the kidney, thereby avoiding secondary operation [23]. Previous studies have reported that magnesium has good biocompatibility and osteogenic stimulation ability [24], and increased bone mass and mineral density were found around magnesium implants in bone indicating that the release of Mg^{2+} ions promote formation of new bone. However, the rapid degradation rate of magnesium and its alloys in contact with body fluids and the rapid release of byproducts (hydroxyl ions and hydrogen) are major problems that urgently require solutions. Porous magnesium has received extensive attention as a biodegradable cancellous bone replacement material since the beginning of this century; it can be absorbed or excreted by the human body, and its mechanical properties are very similar to those of human bones [25].

Porous magnesium scaffolds are manufactured by means of powder metallurgy, laser etching and rapid prototyping. Laser etching can accurately control several parameters, such as porosity, pore diameter and pore diameter distribution, and it exhibits good repeatability [26]. However, the high production cost of this method greatly limits its application in practice. In the rapid prototyping method represented by 3D printing technology [27], a multilayer structure method can be used to prepare porous biocompatible scaffolds with excellent mechanical and bone conduction properties. The combination of 3D images and CT data enables the preparation of 3D bone repair materials that match specific bone defects, resulting in materials with controllable structure, porosity and properties.

In our previous researches [28–31], we developed 3D gel printing (3DGP) and used it to prepare a variety of materials, such as ceramics and metals. In this paper, a Mg scaffold with a controllable pore structure was prepared by the 3DGP method, and its surface was modified with a calcium phosphate coating. A number of studies have shown that the

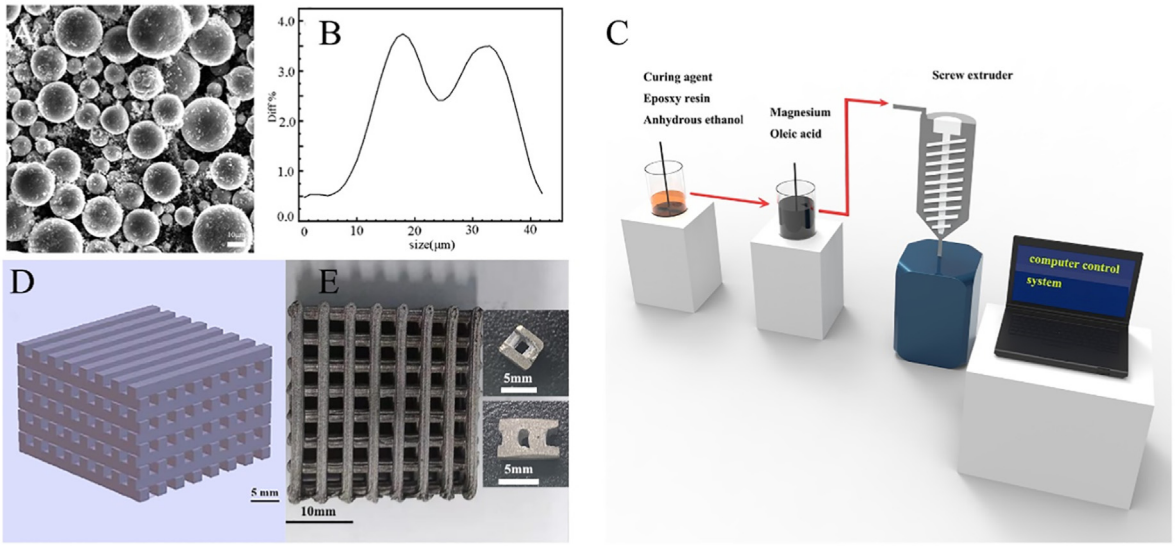

Fig. 1. Preparation of scaffolds (A) SEM image of Mg powder (B) particle size distribution of Mg powder (C) 3D gel printing process flow (D) magnesium scaffold model (E) the sintered body and the final formed scaffold.

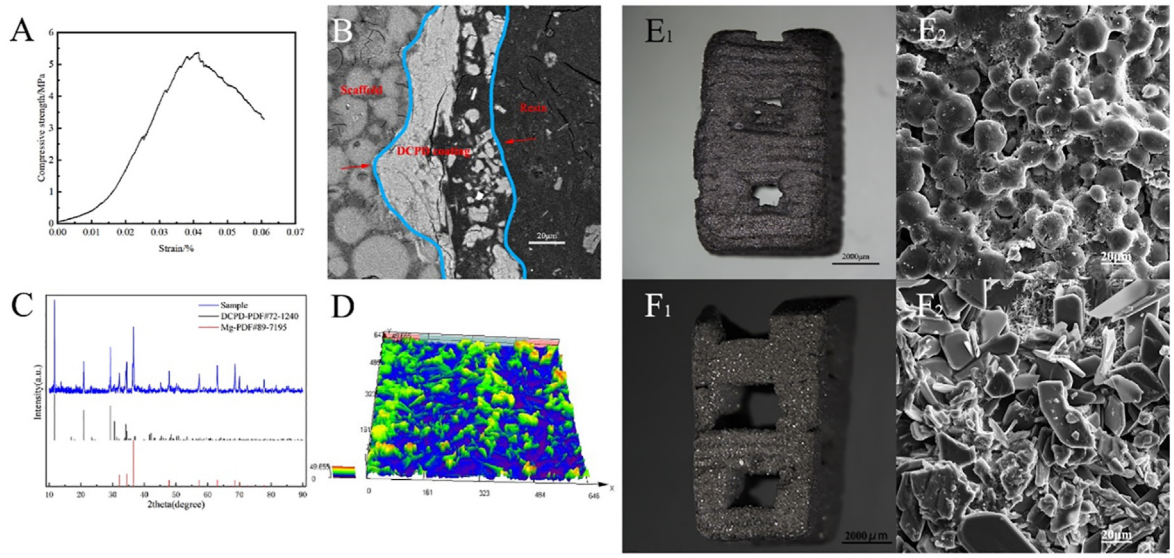

Fig. 2. (A) Compressive strength of sintered Mg scaffold (B) the cross-sectional SEM image of the DCPD coated scaffold, and between the red arrows is the DCPD coating (C)XRD image of DCPD coated Mg scaffold and standard XRD of DCPD and Mg (D) confocal microscope image of the surface of a DCPD coated scaffold (E1) uncoated Mg scaffold (E2) SEM image of E1 (F1) DCPD coated Mg scaffold (F2) SEM image of F1. (For interpretation of the references to color in this figure legend, the reader is referred to the Web version of this article.)

Table 1
Comparison of properties of magnesium scaffolds, TCP scaffolds and cancellous bone.

Physical and mechanical properties	DCPD coated scaffold	β-TCP scaffold	Cancellous bone [36]
Density/g·cm-3	0.72 ± 0.07	1.035	1.8–2.1
Compression modulus/ MPa	5.38 ± 0.87	0.469 ± 0.011	2.08–4.3
Young's modulus/MPa	318 ± 68	54.65 ± 3.41	97.8–134.6
Aperture/mm	2.0 ± 0.1	2.5 mm	0.4–0.6
Porosity/%	57.6 ± 3.9	58.1 ± 6.2	40.0–60.0

addition of DCPD coating on the surface of materials can not only improve biocompatibility and biosafety, but also have excellent osteogenic induction ability, and angiogenic ability [32], and the degradation rate of materials can be effectively controlled by adjusting the thickness of DCPD coating [33,34]. Therefore, we chose to use DCPD coating to modify the surface of the scaffold in this experiment. After the surface modification of the scaffold was completed, the physical properties of the scaffold were systematically analyzed, and its biocompatibility and biosafety were tested in vitro.

2. Materials and methods

2.1. Scaffold preparation and surface modification treatment

2.1.1. Experimental materials

The materials and reagents used in this experiment were: Mg powder (99.8%, Tangshan Weihao Magnesium Powder Co. Ltd.), absolute ethanol (AR, Sinopharm Chemical Reagent Co. Ltd), epoxy resin (AR, Sinopharm Chemical Reagent Co. Ltd) and oleic acid (AR, Sinopharm Chemical Reagent Co. Ltd).

2.1.2. Preparation and properties of slurry

Absolute ethanol and epoxy resin were used as the organic solvent and curing agent, and oleic acid was used as the dispersant. A proper amount of ethanol was used to dissolve the epoxy resin, and then magnesium powder was added. Oleic acid was added in the stirring process as a dispersant. After stirring for a certain time, the slurry was evenly dispersed and could then be used for 3DGP printing. A viscometer was used to test the relationship between slurry viscosity and shear rate. The slurry has the characteristics of a pseudoplastic fluid, and the solids content was 50%.

2.1.3. 3D gel printing process

Fig. 1(C) is the process flow chart of 3D gel printing magnesium scaffold. The scaffold model established by UG was sliced by Cure software and imported into the computer control system. The supplied slurry is loaded into the extrusion device, and the slurry is extruded from the nozzle through the pressure system to obtain the final printed green body. The printed green billet was degreased under the protection of high purity argon gas. After degreasing, it was immediately heated to 570 °C for sintering and held for 1 h.

2.1.4. Properties of sintered scaffolds

The sintered scaffold was tested at 22–23 °C and 40–55% relative humidity. The microstructure of the scaffold was characterized by scanning electron microscopy (SEM, ZEISS EVO®18, Carl ZEISS NTS, Germany). The density of the scaffold material was determined by Archimedes immersion method in absolute ethanol. The compressive strength of the sintered samples was tested by an electronic universal testing machine (CMT5504, SUST Zhuhai) at a loading rate of 0.1 mm/min. The samples used for compressive strength were cut to about 8 mm × 8 mm × 4 mm, then finally grounded with 2000 mesh sandpaper. Three samples were collected for density and compression tests.

2.1.5. Preparation and properties of calcium phosphate coating

The preparation of DCPD was done as follows: appropriate amounts of $NH_4H_2PO_4$ and $Ca(NO_3)_2$ were dissolved in deionized water, and then the oxidized scaffold was immersed in the solution. After standing for a period of time, the scaffold was clamped out, and the appropriate thickness of calcium phosphate coating was obtained on the surface of the scaffold.

DCPD can progressively transform to HA (Hydroxyapatite) in situ via a hydrothermal reaction operating in an alkaline environment. HA is a major component of natural bones. Synthetic HA is considered stable in the physiological environment and exhibits a lower degradation rate than natural HA [35]. DCPD effectively slows the corrosion of the Mg scaffold

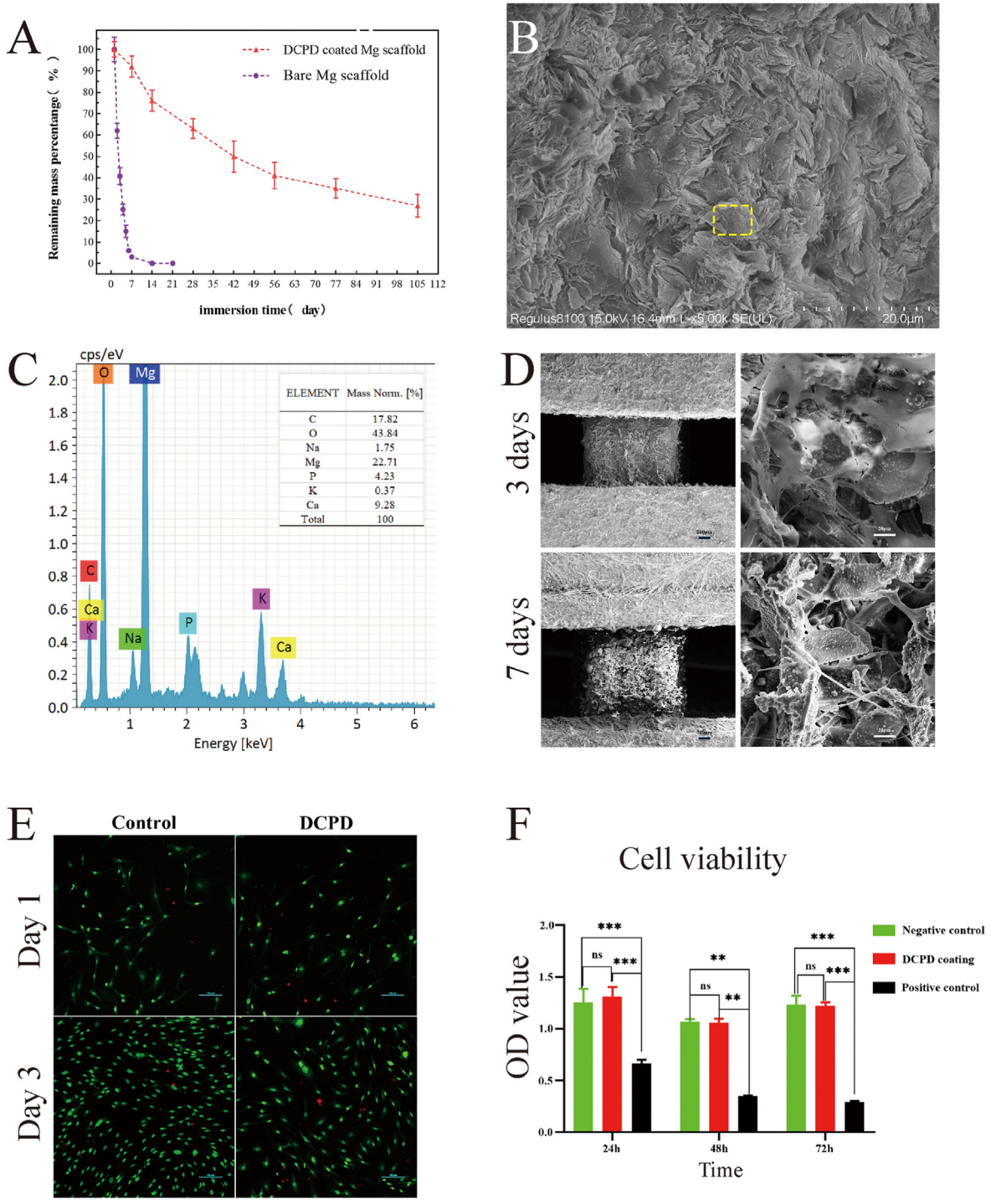

Fig. 3. In vitro experiment (A) Degradation curve in vitro (B): SEM images of DCPD coated magnesium scaffold soaked in SBF for 105 days (C): EDS spectral result in yellow box of (B) (D) Electron microscopic images of DCPD-coated magnesium scaffolds at 3 and 7 days after cell inoculation (E): Alive and dead stain on MC3T3-E1 cells after cultured by DCPD-coated magnesium scaffold extract for 1 day and 3 days (F):24, 48, 72-h CCK-8 cell proliferation detection; CCK-8 cell proliferation test, MC3T3-E1 cells were cultured in scaffold extract 24/48/72 h after the comparison of OD values in the DCPD MG scaffold group (red), negative control group (green) and positive control group (black). It was slightly higher than the negative control at 24H and 48H, and the same at 72H. (For interpretation of the references to color in this figure legend, the reader is referred to the Web version of this article.)

in physiological environments and prolongs the life of the scaffold.

2.2. 2. In vitro degradation experiment

In this experiment, we chose a simulated humoral fluid (SBF) solution to determine degradation behavior. The scaffold was placed in corning tube equipped with SBF, the volume ratio of the scaffold to SBF was 1:60, and the SBF was replaced every 3 days. The experiment was divided into two groups according to the presence or absence of coating, with 30 samples in each group, in a constant temperature water bath at 37 °C. Three scaffolds were removed from each group according to different time points. The scaffolds in each group were immersed in 200 g/L CrO3+10 g/L AgNO3 chromic acid solution configured according to ASTM G1 standard for 1 min to rinse the degradation products on the

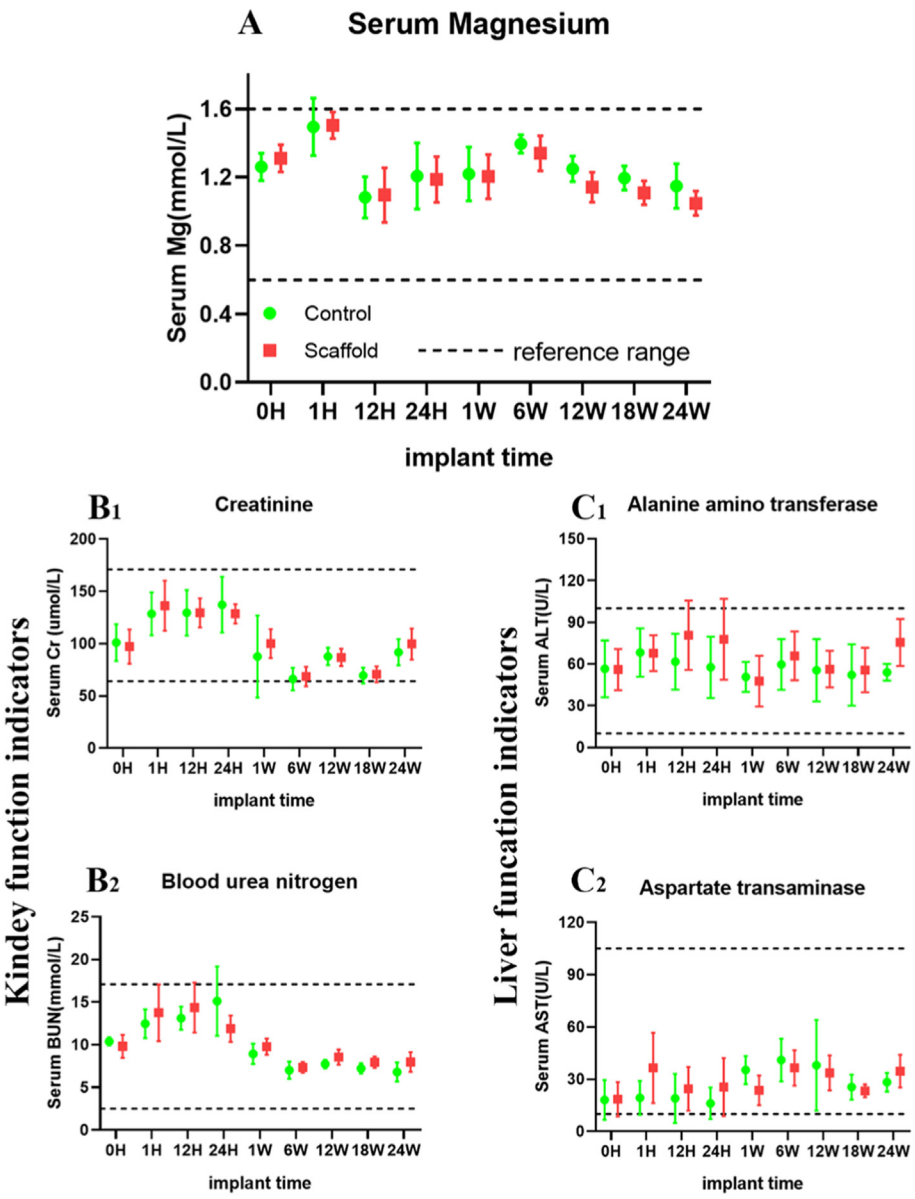

Fig. 4. Biosafety analysis in vivo(A): Serum Mg ion concentration of rabbits in the DCPD MG scaffold group (red) and the control group (green) at different time points. Serum Mg ion concentration in the DCPD MG scaffold group remained at the normal level during the observation time, but was not significantly higher than that in the control group. The results indicated that DCPD Mg scaffolding did not significantly increase the serum Mg concentration(B1) (B2): The changes of serum creatinine (Cr) and urea nitrogen (BUN) in both groups were within the normal range, indicating that renal function was normal after DCPD MG scaffolding(C1) (C2): The serum ALT and AST of the two groups were within the normal reference range, indicating that the liver function of the DCPD MG scaffold group was normal after surgery. (For interpretation of the references to color in this figure legend, the reader is referred to the Web version of this article.)

surface, then washed with anhydrous ethanol, and the weight change was measured after drying at room temperature. The residual magnesium scaffolds soaked in SBF for 105 days were observed by SEM.

2.3. Cytocompatibility evaluation

Mouse-derived osteoblasts (MC3T3-E1, Cell Resource Center of Shanghai Institute for Biological Science, Shanghai, China) were used to test the cellular compatibility of the scaffolds. Dulbecco's Modified Eagle's Medium/Ham's F-12 50/50 Mix with L-Glutamine & 15 mM HEPEs (Corning, USA) was added with 10% feta l bovine serum (Corning, USA) and 1% double antibody (GBICO, Invitrogen Inc.) to the complete medium, which was cultured in an environment of 5% CO_2 and 37 °C. The scaffold was irradiated with cobalt 60 and immersed in the complete medium at 37 °C for 72 h at a ratio of 0.2 g/mL, in accordance with the GBT 16886.5–2003 standard.

2.3.1. Indirect cell cytotoxicity

The cytotoxicity of the extracts was assessed by live/dead staining. MC3T3-E1 cells (5×10^4/well) were seeded into 6-well plates. After 1 day of incubation, the medium was replaced with an extract for 1 and 3 days. Finally, staining was performed with a live/dead kit (Invirtogen) and observed under fluorescence microscopy.

A CCK-8 assay was used to detect cell proliferation activity and cell viability. MTCT3-E1 cells were seeded into 96-well plates at a density of 3×10^3/well and cultured for 24 h. The culture medium was changed, the experimental group used the prepared extract, the negative control group used complete medium, and the positive control group comprised complete medium with 0.1% phenol. Six wells were set in each group and cultured for 1, 2 and 3 days. The medium was discarded at the labeling time, and 100 μl CCK-8 solution (1:9 Medium, Dojindo Laboratories, Japan) was added for 2 h. The absorbance was measured at 450 nm.

2.3.2. Direct cell attachment on the DCPD coated porous magnesium scaffolds

MC3T3-E1 cells (1×10^5 cells/well) were inoculated on the DCPD layer magnesium scaffold. After incubation for 3 and 7 days, the sample was fixed with a 2.5% glutaraldehyde solution and then progressively dehydrated in ethanol. After gold spraying, the sample was observed under field emission scanning electron microscope.

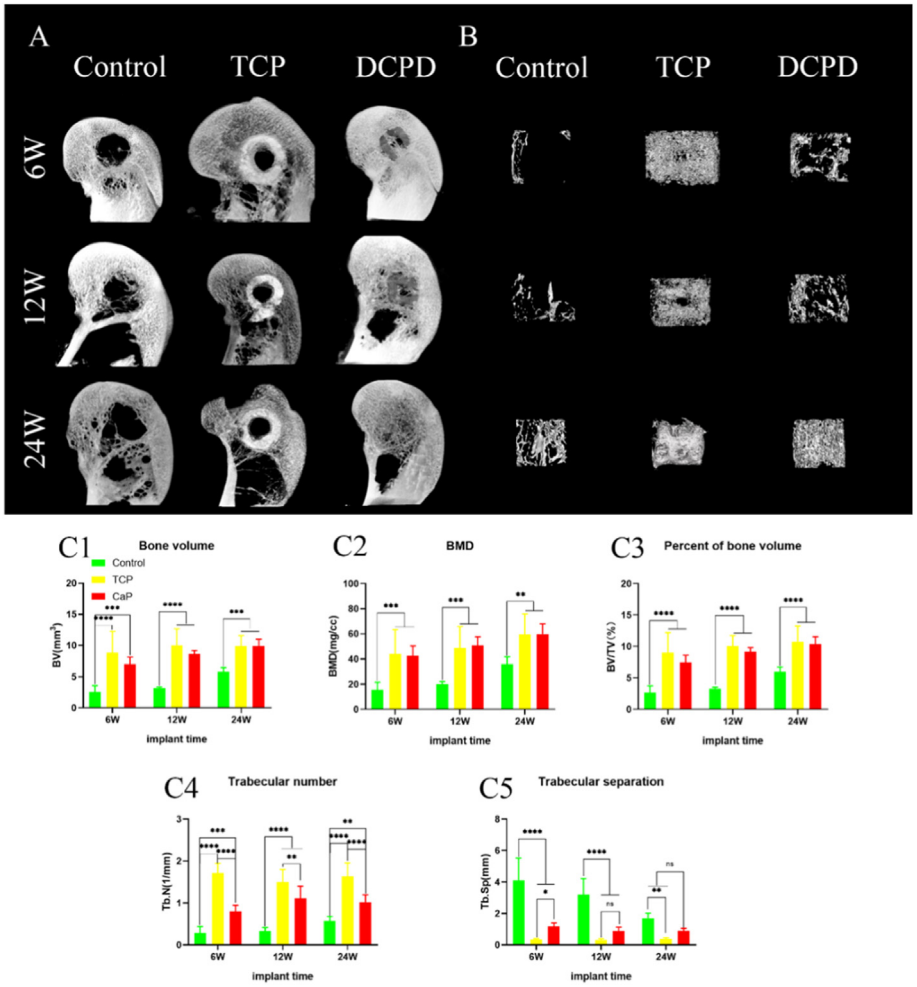

Fig. 5. New bone formation in bone tract. A: Representative micro-CT MIP images at 6, 12, and 24 weeks postoperatively. B: Representative 3D micro-CT images of the region of interest (ROI) with a central diameter of 6 mm at 6, 12, and 24 weeks postoperatively. C: Micro-CT quantitative analysis of new bone in bone tract at 6, 12 and 24 weeks after surgery: BV (C1); Bone Mineral density (C2); BV/TV (C3); Tb.N(C4); Tb. Sp (C5). Each group n = 4 ; #P > 0.05; *P < 0.05; **P < 0.01 ; ***P < 0.005 ; ****P < 0.001.

2.4. Animal model and scaffold implantation

Thirty-six healthy and mature New Zealand white rabbits (male 2–2.5 KG) were selected for animal experiment. This experiment was conducted in accordance with the guidelines for experimental Animals of national Institutes of Health and approved by the Animal Ethics Committee of our hospital. Rabbits were randomly divided into 3 groups, the experimental group was implanted with DCPD-coated magnesium scaffold, the positive control group was implanted with β-TCP scaffold （Wuhan Huawei Biomaterials Engineering Co., LTD.）, and the model group was only drilled for modeling.

The DCPD-coated magnesium scaffold used in the implantation experiment is a cube cut and polished by sintered body, with an aperture of 2X2 mm, an outer diameter of 6 mm, a length and width of 4.24 × 4.24 mm and a height of 7 mm, as shown in Fig. 1(E). After reprocessing, the positive control β-TCP scaffold was 6 mm in diameter, 2.5 mm in aperture and 7 mm in height.

Rabbits were anesthetized with 3% pentobarbital sodium. Then the skin was incised at the lateral condyle of the right distal femur, and the soft tissue was bluntly separated to expose the lateral condyle of femur. Then, an electric drill was used to form a tunnel with a diameter of 6 mm and a depth of about 8 mm on the lateral condyle. The scaffolds were implanted in each group. Finally, the wound was carefully sutured and bandaged after irrigation, and intramuscular penicillin was given 3 days after surgery to prevent infection. The rabbits were killed 6, 12 and 24 weeks after the operation by injecting a pentobarbital sodium overdose through the auricular vein. The femoral condyle was isolated for microscopic CT scan and histological analysis.

2.5. In vivo biosafety tests

Rabbit blood samples were collected before and after surgery at 1, 12, 24h and 1, 6, 12、24 weeks to measure the concentrations of magnesium ions (Mg^{2+}), alanine aminotransferase (ALT), aspartate aminotransferase (AST), creatinine (CR) and blood urea nitrogen (BUN).

2.6. New bone formation and the residue of scaffold

The right femoral condyle was collected and fixed with 4% paraformaldehyde for one week. Then, the distal femurs of the rabbits were scanned by micro-CT with 27 μm spatial resolution. A region of interest (ROI) was selected from the center of the bone tunnel with a diameter of 6 mm and reconstructed using CT analysis software. The images were reconstructed into three-dimensional images and used to measure bone volume density (BV/TV, %), bone mineral density (BMD, mg/cc), trabecular number (Tb. N, 1/mm), and trabecular separation (Tb. Sp, mm).

2.7. Histology analysis

Calcein (10 mg/mL, 15 mg/kg) was injected 14 and 7 days before sampling for fluorescence labeling. The right femoral condyle was collected and fixed with 4% paraformaldehyde for one week. After the completion of CT image scanning, the bone slices were cut into approximately 2 mm slices, soaked in PBS for 1 h, and dehydrated with gradient ethanol solution for the indicated time periods: 50% 24 h, 60% 24 h, 70% 24 h, 80% 24 h, 90% 24 h, 100% 24 h, and 100% 24 h. After that, methyl

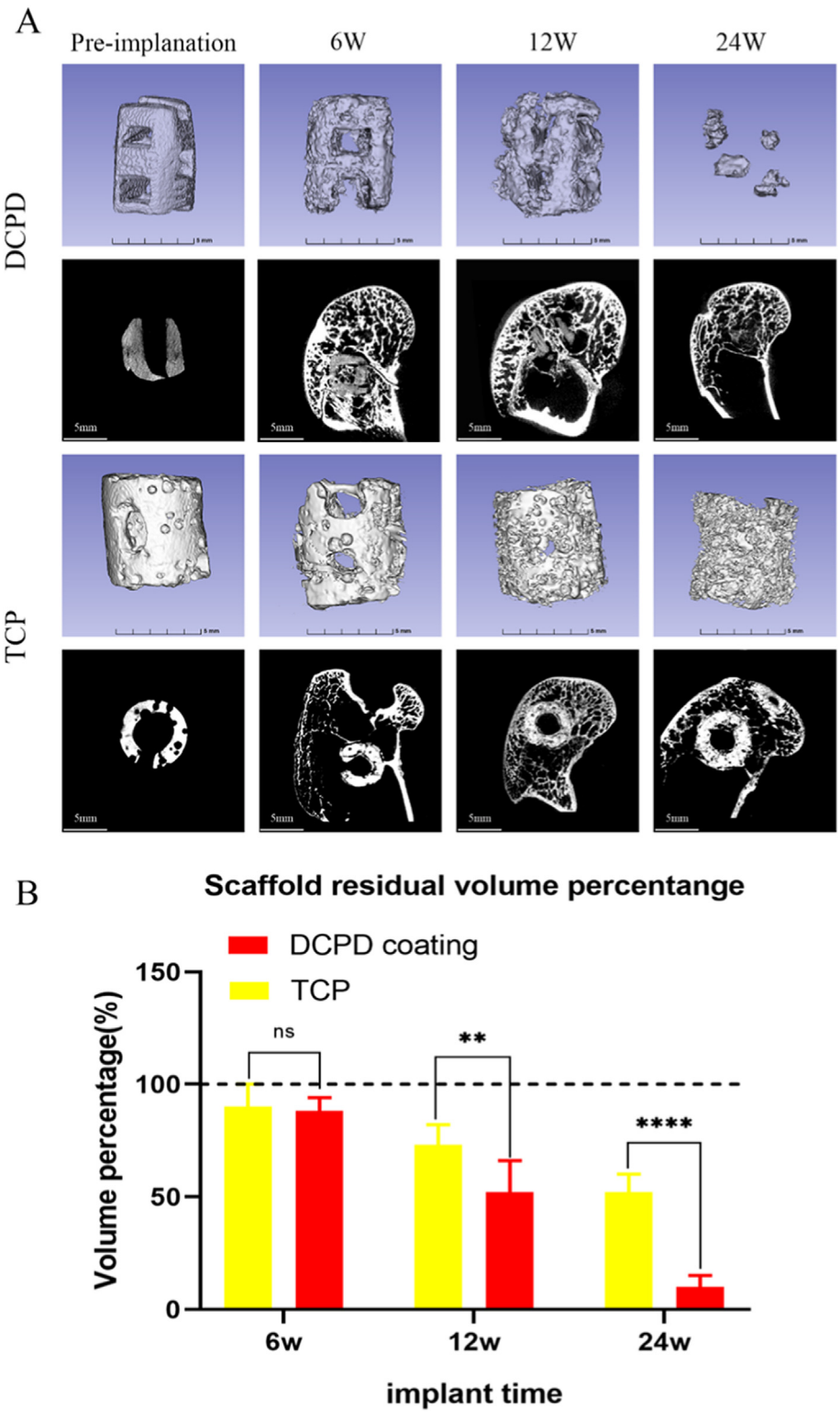

Fig. 6. Degradation of scaffold in vivo. A: residual scaffold in the bony tract at various time points. B: changes in scaffold volume during the process of scaffold degradation in vivo after surgery.

methacrylate resin (Technovit 7200 VLC, Exakt, Germany) was mixed at a 1:1 ratio with 100% ethanol for 24 h, and then soak it in 100% methyl methacrylate resin for 4 h twice. The samples were then embedded in methyl methacrylate resin. The embedded samples were sliced using Arc-Oscillation (Exakt) units and then ground to a final thickness of 20 μm. First, the unstained sections were observed under a fluorescence microscope (BX51, Olympus, Japan), analyzed and photographed as evidence of bone regeneration. Bone histological analysis was performed using Masson-Goldner staining and then observed with a BX51 microscope under normal light. The collected data were analyzed using Bioquant Osteo (Bioquant Image Analysis Corporation) software.

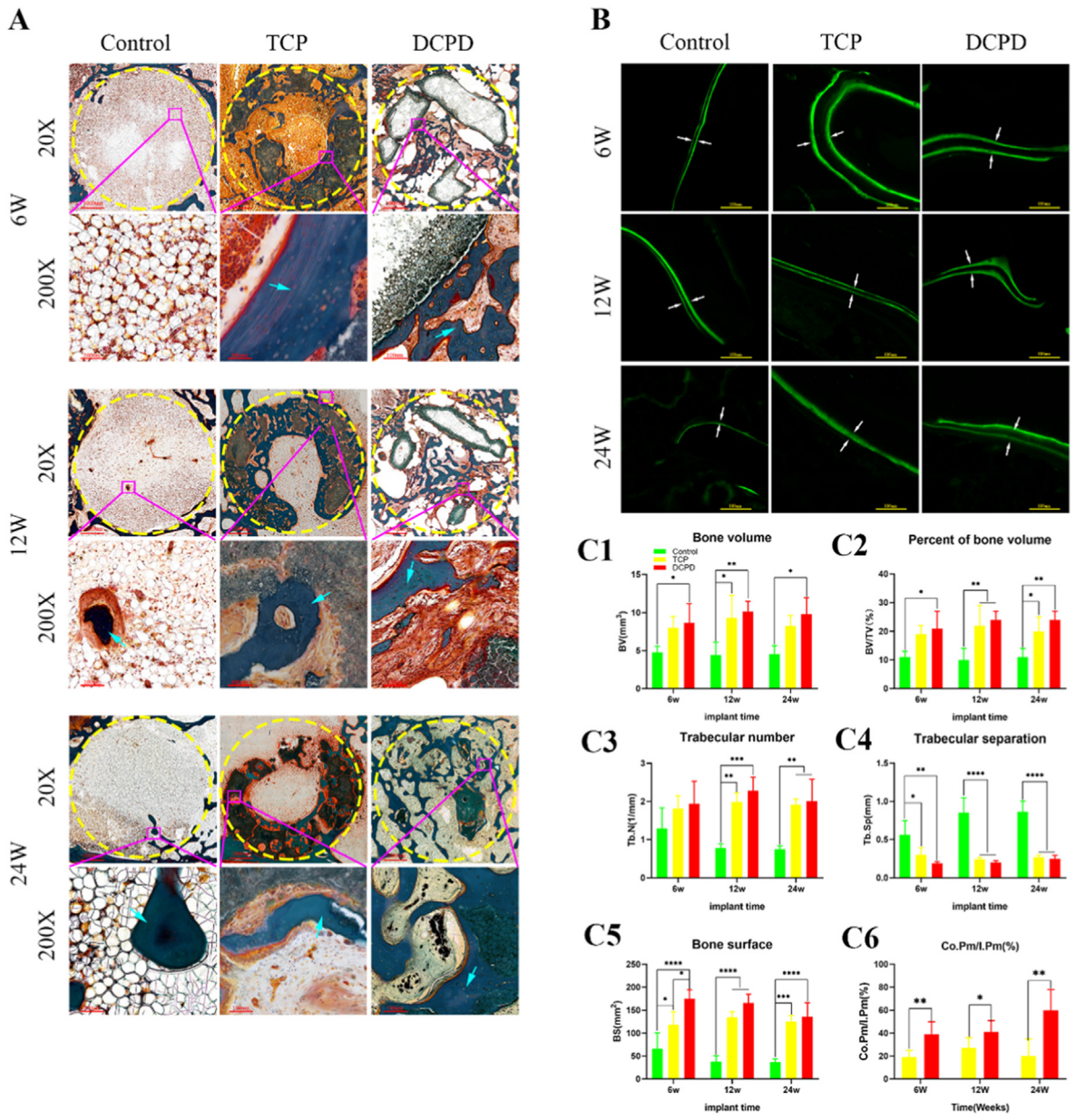

Fig. 7. Histological analysis of bone formation after scaffold implantation.: A: Histological analysis of non-decalcified bone tissue sections. Masson-Goldner staining shows new bone with blue arrows. B: Fluorescence micrograph of undecalcified sections. The white arrows indicate new bone areas. C1–C6: Quantitative analysis of new bone formation (BV, BV/TV, Tb.N, Tb. Sp, BS, Co.Pm/I.Pm), bone formation 6, 12 and 24 weeks after scaffold implantation. N = 3 #P > 0.05 for each group; *P < 0.05. (For interpretation of the references to color in this figure legend, the reader is referred to the Web version of this article.)

2.8. Statistical analysis

All data were analyzed using SPSS 17.0 software. All results are expressed as means with standard errors. Two-way-ANOVA was used for statistical analysis. P values < 0.05 indicate that the difference is statistically significant.

3. Result

3.1. Preparation and characterization of scaffolds

As shown in Fig. 1(A), the Mg powder used in this study was produced by inert gas atomization, and its particle shape was spherical. The average particle size (D50) of Mg powder was approximately 31.10 μm, and the particle size distribution of the Mg powder is shown in Fig. 1(B). Fig. 1 (D) shows the magnesium scaffold model established by UG (Unigraphics NX) , and Fig. 1 (E) shows the sintered magnesium scaffold and on the right is the experimental implant scaffold cut from the sintered body. The scaffold size was 24 mm × 24 mm × 15 mm. The strength of a scaffold is affected by many factors. Imperfections during printing or sintering can reduce its compressive strength. In general, the strength of the scaffold can reach 5–10 MPa. Fig. 2(A) shows the compressive strength of the magnesium scaffold used in this experiment, which was 5.38 MPa. Table 1 shows the comparison of mechanical properties of representative DCPD porous magnesium scaffolds and human cancellous bone.

The physical and SEM images of the pure Mg scaffold and DCPD-coated Mg scaffold are shown in Fig. 2(E) (F). Fig. 2(B) shows the electron microscope image of cross section of DCPD coated scaffold. The average thickness of the coating measured is 41.75 ± 12.30 μm. Fig. 2(C) shows an XRD image of a DCPD-coated Mg scaffold.

3.2. In vitro study

In vitro degradation experiment, the uncoated porous magnesium scaffold completely degraded after approximately 1 weeks, and the DCPD-coated porous magnesium scaffold still had approximately 20% residual left after 20 weeks (Fig. 3(A)). Fig. 3(B) shows the surface morphology of DCPD-coated magnesium scaffold soaked in SBF solution for 105 days. In this figure, it is hard to see the magnesium scaffold base, and the surface is completely covered by lamellar (or needle-like) crystals. According to EDS energy spectrum data (Fig. 3(C)) and other research results, it is judged as HA crystal [12,35]. This indicates that after DCPD-coated magnesium scaffolds are soaked in SBF solution for a long time, a large amount of HA can be deposited on the surface of scaffolds. A large amount of HA deposition on the surface of scaffolds hinders the further corrosion of magnesium scaffolds by SBF and delays the degradation rate of magnesium scaffolds.

A typical SEM image of the cells on the scaffold is shown in Fig. 3 (D). After 3 days of culture, the cells were firmly attached to the scaffold coating surface, and the number of cells was significantly expanded on the 7th day. DCPD coating showed good cell adhesion.

As shown in Fig. 3 (E), there was no significant difference in the live/dead staining of the scaffold extract between the experimental group and the control group. CCK-8 test further confirmed the previous results, as shown in Fig. 3 (F), the cell viability of MC3T3-E1 cells did not differ significantly from that of the control group after cultured in the extract 24/48/72 h.

3.3. In vivo biosafety tests

Serum magnesium ion levels and blood biochemical indexes were analyzed 0–24 weeks after implantation in vivo. During the observation time, the serum Mg ion concentration in the DCPD group remained at the normal level but was not significantly higher than that of the control group, indicating that the serum Mg ion concentration was not significantly increased after implanting Mg scaffold with DCPD coating (Fig. 4). Fig. 4(A) shows the changes in serum Mg ion concentration at 0, 1, 12, and 24 h after surgery and at 1, 6, 12, and 24 weeks after surgery. There was no significant difference ($p > 0.05$, $n = 3$). There were no abnormal changes in biochemical indexes during scaffold implantation. The renal function indexes of the two groups were creatinine (Cr) (B1) and blood urea nitrogen (BUN) (B2) at different time points. Alanine aminotransferase (ALT) (C1) and ascorbic aminotransferase (AST) (C2) were in the normal range. These results indicate that DCPD-coated 3D-printed pure magnesium scaffolds exhibit good biosafety in vivo.

3.4. New bone formation and the residue of scaffold

In the rabbit femoral condyle defect experiment, we analyzed the formation of new bone in the defect area by micro-CT. As shown in Fig. 5(A), radiography confirmed that at 6, 12, and 24 weeks postoperatively, there was more bone formation in the bone defect area in the DCPD group than in the control group, and the level was comparable to that in the TCP group. The formation of new bone in the micro-CT reconstruction tunnel of the bone defect is shown in Fig. 5(B). At 6, 12 and 24 weeks after surgery, more new bone was formed in the DCPD group and the TCP group than in the control group. As shown in Fig. 5(C), the indexes of BV, BMD and BV/TV in the DCPD group were roughly equal to those in the TCP group. However, there were significant differences between the DCPD group and the TCP group in Tb. N and Tb. Sp indexes; this was largely related to the fact that the material density of TCP was very close to that of bone, which prevented micro-CT from distinguishing them effectively.

In vivo degradation of the scaffold is shown in Fig. 6. After micro-CT three-dimensional reconstruction of preoperative and postoperative 6 weeks, 12 weeks and 24 weeks DCPD coated Mg scaffolds and β-TCP scaffolds (Fig. 6(A)), the residual volume fractions of scaffolds were obtained, and statistical analyses were performed (Fig. 6(B)). At 6 weeks, the scaffold degradation of the two groups was similar, but there was a significant difference between the two groups at 12 weeks and 24 weeks.

3.5. Histology analysis

The histological evaluation of new bone towns in the bone tract is shown in Fig. 7. Newly formed bone tissue in the defect area at 6, 12, and 24 weeks after scaffold implantation is shown in Fig. 7(A). Fig. 7(A) shows that the bone tunnel in the control group was filled with adipocytes, and there were few osteocytes at 6, 12 and 24 weeks after surgery. However, bone tissue was formed in the TCP group and the DCPD group at 6 weeks after surgery, but the morphology of osteogenesis was slightly different. The central hole of the TCP scaffold was filled with adipocytes, and bone tissue was formed around the scaffold. Bone tissue had grown into the central hole of the DCPD scaffold. At 24 weeks, most of the scaffolds in the DCPD group had been degraded, and the bone tissue still maintained osteogenic activity. A large number of osteoblasts and osteoid cells were visible, and the morphology of the bone tract area was close to that of the preoperative state. Fig. 7(B) shows calcein-labeled osteogenic activity. DCPD group still had relatively active osteogenic activity at 24 weeks. Fig. 7(C) shows the BV obtained by Bioquant Osteo2020 analysis. It can be seen that the DCPD-coated magnesium scaffold group has similar results with β-TCP in most indicators (BV,BS,BV/TV, Tb. N and Tb. Sp) , and is significantly better than the β-TCP group in bone bonding rate (Co.Pm/I.Pm).

4. Discussion

Several factors should be considered in the design of bone grafts. First, a porous structure with a sufficient pore size to allow the exchange of bone cells, nutrients and metabolites. It is generally accepted that a pore size greater than 300 μm is suitable for the formation of blood vessels and new bone [37–40]. Second, there should be a surface that allows blood vessels to grow, bone cells to attach, migrate, and proliferate. Third, sufficient mechanical properties are essential to withstand loads from surrounding tissues. Fourth, controllable biodegradability allows the tissue to be replaced gradually. Finally, good biocompatibility is indispensable.

In this study, magnesium particles were used as raw materials to directly prepare porous magnesium scaffolds by 3D gel printing method, and DCPD coating was prepared on the surface of scaffolds. The mechanical properties, biocompatibility, degradation rate and osteogenic ability of the scaffolds were studied by in vitro and in vivo experiments. The compressive strength of β-TCP porous scaffolds was generally below 10 MPa [36,41–43], and that of the commercial β-TCP implants we used in the positive control group was greater than or equal to 4 MPa. The compressive strength and porosity of the DCPD-coated porous magnesium scaffold prepared in this study are 5.38 ± 0.87 MPa and 57.6 ± 3.9%. As shown in the density of magnesium scaffold is slightly lower than that of cancellous bone, and its compressive strength and elastic modulus are higher than that of cancellous bone, which can play a supporting role. Moreover, the porosity of magnesium scaffold is similar to that of cancellous bone, and its pore size is larger than that of cancellous bone, which is conducive to the growth of neovascularization bone tissue.

Degradation of Mg and its alloy in aqueous solution is caused by the following electrochemical reaction [44]:

$$\text{Anodic reaction}: \quad Mg \rightarrow Mg^{2+} + 2e \tag{1}$$

$$\text{Cathodic reaction}: \quad 2H_2O + 2e \rightarrow H_2 + 2OH^- \tag{2}$$

$$\text{Overall reaction}: \quad Mg + 2H_2O \rightarrow Mg(OH)_2 + H_2 \tag{3}$$

Based on the above reactions, the main component of the corrosion

layer on the magnesium surface is thought to be magnesium hydroxide, which has a low solubility in water and protects the magnesium substrate. Only when chloride ion concentration exceeds 30mmol/L in the environment, magnesium hydroxide begins to transform from refractory magnesium hydroxide to soluble magnesium chloride, leading to serious corrosion of magnesium matrix [45]. DCPD coating reduces the degradation rate of magnesium by reducing its contact with liquid. Studies have shown that DCPD coating significantly reduces the speed of Mg–Mn–Zn alloy in SBF [46]. However, compared with other calcium-phosphorus coatings, THE protective effect of DCPD is relatively weak. Some studies have shown that the protective effect of DCPD is weaker than that of HA, FHA and Monetite coatings [47–49]. The degradation process of DCPD in vivo may be divided into two stages. In the initial stage, DCPD is mainly degraded by hydrolysis [50], which makes the DCPD coating loose, and in the later stage, it is decomposed and absorbed by the body under the action of osteoclasts [51]. On the other hand, the relatively fast degradation rate of DCPD coating compared with other coatings such as HA can also avoid the long-term existence of implants in the body. In vitro experiments, compared with uncoated scaffolds, DCPD coating significantly slowed down the degradation rate of scaffolds, which is consistent with previous studies [52, 53]. However, the degradation rate of scaffolds was slightly different in vivo and in vitro. In vivo, the scaffold achieved the same level of weightlessness for six weeks longer than in vitro. This suggests that DCPD coating is more effective in slowing the rate of degradation in the body. We believe that the long-term presence of scaffolds in a liquid environment is a reasonable reason for in vitro experiments. The DCPD coating in the body cuts off most of the magnesium's contact area with the blood, reducing the corrosion rate. After the hematoma mechanization stage, the scaffold was not completely immersed in liquid in the internal environment as it was in vitro, thus reducing the degradation rate of the scaffold. In the in vitro biocompatibility test, the well-grown cells were observed on the scaffold under SEM, and no significant difference was found in the live/dead staining compared with the control group. CCK-8 test further confirmed the above conclusion. Some studies have found that magnesium scaffolds can cause better cell attachment, growth and proliferation [54], but this phenomenon has not been observed in this study. The reduction of Mg ion release caused by DCPD coating should be considered as a reason.

In vivo experiments, the change of magnesium ion concentration in vivo is the key point of our concern. The results showed that magnesium ions increased significantly 1h after the operation, which may be related to the slight damage to the coating during the implantation of the scaffold. In general, the concentration of magnesium ions fluctuated within the normal range during the experiment period. No abnormalities of liver or kidney function was observed.

In order to facilitate the fabrication, the scaffold in this study adopts the aperture and cuboid structure of 2 mm. Although the maximum contact area with bone was not achieved, the results were still better than β-TCP control group. In the β-TCP group, the central cavity of the TCP scaffold did not achieve complete bone growth at all time points. However, in the magnesium scaffold group, bone tissue regeneration was observed in the central hole at 6th week and the residual part of the scaffold was completely wrapped by bone tissue at 24th week, showing good osteoinduction, osteoconduction and histocompatibility.

5. Conclusion

In this study, we designed and manufactured a porous scaffold composed of pure magnesium particles and coated with DCPD coating using 3D gel printing technology. Porosity and pore size can be controlled independently and accurately. The DCPD coated pure granular scaffold has suitable initial mechanical properties, good biocompatibility, and suitable degradation rate, which stimulates bone regeneration and mediates new bone formation and remodeling.

Credit author statement

Yuxuan Zhang, Tao Lin, Haoye Meng: Methodology, Investigation, Formal analysis, Writing – original draft. Xueting Wang: Methodology. Hong Peng: Writing – review & editing. Guangbo Liu: Methodology. Shuai Wei: Methodology. Qiang Lu, Wenjing Xu: Funding acquisition. Yu Wang, Aiyuan Wang: Writing – review & editing, Huiping Shao: Conceptualization, Writing – review & editing, Resources, Supervision, Funding acquisition. Jiang Peng: Resources, Validation, Supervision.

Declaration of competing interest

The authors declare that they have no known competing financial interests or personal relationships that could have appeared to influence the work reported in this paper.

Acknowledgements

This study was supported by National Key R&D Plan of China (2016YFC1102104).

References

[1] Chen J-p, Zhang F. Advanced research on treatment for bony defect. China J Orthopaed Traumatol 2004;12.
[2] Faour O, Dimitriou R, Cousins CA, Giannoudis PV. The use of bone graft substitutes in large cancellous voids: any specific needs? Injury 2011;42:S87–90.
[3] Greenwald AS, Boden SD, Goldberg VM, Khan Y, Laurencin CT, Rosier RN. Bone-graft substitutes: facts, fictions, and applications. JBJS 2001;83(2):S98–103.
[4] Bauer TW, Muschler GF. Bone graft materials: an overview of the basic science. Clin Orthop Relat Res 2000;371:10–27.
[5] Ahlmann E, Patzakis M, Roidis N, Shepherd L, Holtom P. Comparison of anterior and posterior iliac crest bone grafts in terms of harvest-site morbidity and functional outcomes. JBJS 2002;84(5):716–20.
[6] St John TA, Vaccaro AR, Sah AP, Schaefer M, Berta SC, Albert T, et al. Physical and monetary costs associated with autogenous bone graft harvesting. Am J Orthoped 2003;32(1):18–23.
[7] Finkemeier CG. Bone-grafting and bone-graft substitutes. JBJS 2002;84(3):454–64.
[8] Lin FH, Liao CJ, Chen KS, Sun JS, Lin CY. Preparation of βTCP/HAP biphasic ceramics with natural bone structure by heating bovine cancellous bone with the addition of $(NH_4)_2HPO_4$. J Biomed Mate Res: Offic J Soc Biomater, Japanese Soc Biomater Australian Soc Biomater Korean Soc Biomater 2000;51(2):157–63.
[9] Baldwin P, Li DJ, Auston DA, Mir HS, Yoon RS, Koval KJ. Autograft, allograft, and bone graft substitutes: clinical evidence and indications for use in the setting of orthopaedic trauma surgery. J Orthop Trauma 2019;33(4):203–13.
[10] Li H, Lin K, Chang J. Preparation of macroporous polymer scaffolds using calcined cancellous bone as a template. J Biomater Sci Polym Ed 2005;16(5):575–84.
[11] Pattanayak DK, Fukuda A, Matsushita T, Takemoto M, Fujibayashi S, Sasaki K, et al. Bioactive Ti metal analogous to human cancellous bone: fabrication by selective laser melting and chemical treatments. Acta Biomaterialia 2011;7(3):1398–406.
[12] Li J, Cao F, Wu B, Yang J, Xu W, Wang W, et al. Immobilization of bioactive vascular endothelial growth factor onto Ca-deficient hydroxyapatite-coated Mg by covalent bonding using polydopamine. J Orthop Translat 2021;30:82–92. https://doi.org/10.1016/j.jot.2021.06.002. Epub 2021/10/19. PubMed PMID: 34660198; PubMed Central PMCID: PMCPMC8487887.
[13] Trombelli L, Simonelli A, Pramstraller M, Wikesjö UM, Farina R. Single flap approach with and without guided tissue regeneration and a hydroxyapatite biomaterial in the management of intraosseous periodontal defects. J Periodontol 2010;81(9):1256–63.
[14] Pina S, Oliveira JM, Reis RL. Natural-based nanocomposites for bone tissue engineering and regenerative medicine: a review. Adv Mater 2015;27(7):1143–69.
[15] Atak BH, Buyuk B, Huysal M, Isik S, Senel M, Metzger W, et al. Preparation and characterization of amine functional nano-hydroxyapatite/chitosan bionanocomposite for bone tissue engineering applications. Carbohydr Polym 2017;164:200–13.
[16] Fukuda N, Tsuru K, Mori Y, Ishikawa K. Fabrication of self-setting β-tricalcium phosphate granular cement. J Biomed Mater Res B Appl Biomater 2018;106(2):800–7.
[17] Castro AG, Polini A, Azami Z, Leeuwenburgh SC, Jansen JA, Yang F, et al. Incorporation of PLLA micro-fillers for mechanical reinforcement of calcium-phosphate cement. J Mech Behav Biomed Mater 2017;71:286–94.
[18] Ding Y, Li W, Müller T, Schubert DW, Boccaccini AR, Yao Q, et al. Electrospun polyhydroxybutyrate/poly (ε-caprolactone)/58S sol–gel bioactive glass hybrid scaffolds with highly improved osteogenic potential for bone tissue engineering. ACS Appl Mater Interfaces 2016;8(27):17098–108.
[19] Kalita SJ, Bose S, Hosick HL, Bandyopadhyay A. Development of controlled porosity polymer-ceramic composite scaffolds via fused deposition modeling. Mater Sci Eng C 2003;23(5):611–20.

[20] Li JP, de Wijn JR, Van Blitterswijk CA, de Groot K. Porous Ti6Al4V scaffold directly fabricating by rapid prototyping: preparation and in vitro experiment. Biomaterials 2006;27(8):1223–35.
[21] Strąkowska P, Beutner R, Gnyba M, Zielinski A, Scharnweber D. Electrochemically assisted deposition of hydroxyapatite on Ti6Al4V substrates covered by CVD diamond films—coating characterization and first cell biological results. Mater Sci Eng C 2016;59:624–35.
[22] Ghali E, Dietzel W, Kainer K-U. General and localized corrosion of magnesium alloys: a critical review. J Mater Eng Perform 2004;13(1):7–23.
[23] Hänzi AC, Gerber I, Schinhammer M, Löffler JF, Uggowitzer PJ. On the in vitro and in vivo degradation performance and biological response of new biodegradable Mg–Y–Zn alloys. Acta Biomater 2010;6(5):1824–33.
[24] Zhang Y, Xu J, Ruan YC, Yu MK, O'Laughlin M, Wise H, et al. Implant-derived magnesium induces local neuronal production of CGRP to improve bone-fracture healing in rats. Nat Med 2016;22(10):1160–9.
[25] Staiger MP, Pietak AM, Huadmai J, Dias G. Magnesium and its alloys as orthopedic biomaterials: a review. Biomaterials 2006;27(9):1728–34.
[26] Geng F, Tan L, Zhang B, Wu C, He Y, Yang J, et al. Study on β-TCP coated porous Mg as a bone tissue engineering scaffold material. J Mater Sci Technol 2009;25(1):123–9.
[27] Brunello G, Sivolella S, Meneghello R, Ferroni L, Gardin C, Piattelli A, et al. Powder-based 3D printing for bone tissue engineering. Biotechnol Adv 2016;34(5):740–53.
[28] Ren X, Shao H, Lin T, Zheng H. 3D gel-printing—an additive manufacturing method for producing complex shape parts. Mater Des 2016;101:80–7.
[29] Shao H, Zhao D, Lin T, He J, Wu J. 3D gel-printing of zirconia ceramic parts. Ceram Int 2017;43(16):13938–42.
[30] Shao H, He J, Lin T, Zhang Z, Zhang Y, Liu S. 3D gel-printing of hydroxyapatite scaffold for bone tissue engineering. Ceram Int 2019;45(1):1163–70.
[31] Yang T, Tamaddon M, Jiang L, Wang J, Liu Z, Liu Z, et al. Bilayered scaffold with 3D printed stiff subchondral bony compartment to provide constant mechanical support for long-term cartilage regeneration. J Orthop Translat 2021;30:112–21. https://doi.org/10.1016/j.jot.2021.09.001. Epub 2021/11/02. PubMed PMID: 34722154; PubMed Central PMCID: PMCPMC8526903.
[32] Malhotra A, Habibovic P. Calcium phosphates and angiogenesis: implications and advances for bone regeneration. Trends Biotechnol 2016;34(12):983–92.
[33] Wei WA, Gjb D, Qw A, Hua H, Xl A, Hui ZD, et al. The in vitro and in vivo biological effects and osteogenic activity of novel biodegradable porous Mg alloy scaffolds. Mater Des.189.
[34] Guan X, Xiong M, Zeng F, Xu B, Yang L, Guo H, et al. Enhancement of osteogenesis and biodegradation control by brushite coating on Mg-Nd-Zn-Zr alloy for mandibular bone repair. ACS Appl Mater Interfaces 2014;6(23):21525–33. https://doi.org/10.1021/am506543a. Epub 2014/10/25. PubMed PMID: 25343576.
[35] Eliaz N, Metoki N. Calcium phosphate bioceramics: a review of their history, structure, properties, coating technologies and biomedical applications. Materials 2017;10(4):334.
[36] Wähnert D, Hoffmeier KL, Stolarczyk Y, Fröber R, Hofmann GO, Mückley T. Evaluation of a customized artificial osteoporotic bone model of the distal femur. J Biomater Appl 2011;26(4):451–64.
[37] Karageorgiou V, Kaplan D. Porosity of 3D biomaterial scaffolds and osteogenesis. Biomaterials 2005;26(27):5474–91.
[38] Murphy CM, Haugh MG, O'brien FJ. The effect of mean pore size on cell attachment, proliferation and migration in collagen–glycosaminoglycan scaffolds for bone tissue engineering. Biomaterials 2010;31(3):461–6.
[39] Saito E, Saito A, Kuboki Y, Kimura M, Honma Y, Takahashi T, et al. Periodontal repair following implantation of beta-tricalcium phosphate with different pore structures in class III furcation defects in dogs. Dent Mater J 2012;31(4):681–8.
[40] Ai C, Lee YHD, Tan XH, Tan SHS, Hui JHP, Goh JC. Osteochondral tissue engineering: perspectives for clinical application and preclinical development. J Orthop Translat 2021;30:93–102. https://doi.org/10.1016/j.jot.2021.07.008. Epub 2021/11/02. PubMed PMID: 34722152; PubMed Central PMCID: PMCPMC8517716.
[41] Lim H-K, Hong S-J, Byeon S-J, Chung S-M, On S-W, Yang B-E, et al. 3D-Printed ceramic bone scaffolds with variable pore architectures. Int J Mol Sci 2020;21(18):6942.
[42] Kang H-J, Makkar P, Padalhin AR, Lee G-H, Im S-B, Lee B-T. Comparative study on biodegradation and biocompatibility of multichannel calcium phosphate based bone substitutes. Mater Sci Eng C 2020;110:110694.
[43] Okanoue Y, Ikeuchi M, Takemasa R, Tani T, Matsumoto T, Sakamoto M, et al. Comparison of in vivo bioactivity and compressive strength of a novel superporous hydroxyapatite with beta-tricalcium phosphates. Arch Orthop Trauma Surg 2012;132(11):1603–10.
[44] Song GL, Atrens A. Corrosion mechanisms of magnesium alloys. Adv Eng Mater 2010;1(1):11–33.
[45] Witte F, Hort N, Vogt C, Cohen S, Feyerabend F. Degradable biomaterials based on magnesium corrosion. Curr Opin Solid State Mater Sci 2008;12(5):63–72.
[46] Xu L, Zhang E, Ke Y. Phosphating treatment and corrosion properties of Mg-Mn-Zn alloy for biomedical application. J Mater Sci Mater Med 2009;20(4):859–67.
[47] Yang S, Zhang S, Li J, Zhao C, Zhang X. Electrodeposition of Ca-P coatings on biodegradable Mg alloy: in vitro biomineralization behavior. Acta Biomaterialia 2010;6(5):1736–42.
[48] Shadanbaz S, Walker J, Staiger MP, Dias GJ, Pietak A. Growth of calcium phosphates on magnesium substrates for corrosion control in biomedical applications via immersion techniques. J Biomed Mater Res B Appl Biomater 2013;101b(1):162–72.
[49] Shadanbaz S, Walker J, Woodfield TBF, Staiger MP, Dias GJ. Monetite and brushite coated magnesium: in vivo and in vitro models for degradation analysis. J Mater Sci Mater Med 2014;25(1):173–83.
[50] Theiss F, Apelt D, Brand B, Kutter A, Zlinszky K, Bohner M, et al. Biocompatibility and resorption of a brushite calcium phosphate cement. Biomaterials 2005;26(21):4383–94.
[51] Kuemmerle JM, Oberle A, Oechslin C, Bohner M, Frei C, Boecken I, et al. Assessment of the suitability of a new brushite calcium phosphate cement for cranioplasty - an experimental study in sheep. J Cranio-Maxillo-Fac Surg 2005;33(1):37–44.
[52] Gao J, Su Y, Qin Y-X. Calcium phosphate coatings enhance biocompatibility and degradation resistance of magnesium alloy: correlating in vitro and in vivo studies. Bioactive Materials 2021;6(5):1223–9.
[53] Rahim MI, Tavares A, Evertz F, Kieke M, Seitz JM, Eifler R, et al. Phosphate conversion coating reduces the degradation rate and suppresses side effects of metallic magnesium implants in an animal model. J Biomed Mater Res B Appl Biomater 2017;105(6):1622–35.
[54] Lai Y, Li Y, Cao H, Long J, Wang X, Li L, et al. Osteogenic magnesium incorporated into PLGA/TCP porous scaffold by 3D printing for repairing challenging bone defect. Biomaterials 2019;197:207–19.